

# Inhomogeneous Absorbers and Derived Column Densities

Bassem M. Sabra

American University of Science and Technology, P. O. Box 95, Zahle, LEBANON

Fred Hamann

Department of Astronomy, University of Florida, Gainesville, FL 32611, USA

*ApJ*, submitted

## ABSTRACT

We study the dependence of column densities derived from absorption lines on the spatial distribution of the ions in an absorber. In particular, we investigate four varieties of coverage by the absorber of the background source: the familiar homogeneous partial coverage (HPC), and three functional forms that parameterize inhomogeneous coverage: a powerlaw, an ellipse quadrant, and a Gaussian distribution. We calculate the residual line intensities obtained from our inhomogeneous coverage models and then use these intensities as “observed” quantities to compute the optical depth and covering factors assuming HPC. We find that the resulting spatially-averaged optical depths are comparable (within a factor of  $\lesssim 1.5$ ) to the average optical depths of the input distributions, as long as the input distributions do not contain spatially narrow “spikes.” Such spikes (very large optical depths over a small coverage area) can profoundly affect the average optical depth in the absorber but have little impact on the observed intensities. We also study the converse approach: we start with HPC as the assumed physical model and then infer the parameters of the inhomogeneous coverage models through a doublet analysis. Again the resulting average optical depths are comparable to the corresponding quantity of the input distribution. Finally, we construct a more realistic two-dimensional optical depth distribution based on a random distribution of absorbing clouds, and we use that to calculate observed intensities. A doublet analysis applied to those intensities shows all four of our simple analytic functions yield an accurate estimate of the true average optical depth, while the powerlaw yields the best approximation to the initial distribution.

*Subject headings:* line: formation— absorption lines—radiative transfer —quasars

## 1. Introduction

Resonant absorption lines observed in the spectra of many astronomical objects provide important diagnostics about the physical and chemical states of the environments in which they originate. One of the important aims of absorption line studies is determining accurate elemental abundances. The steps involved in using absorption lines as abundance diagnostics are the following: Derive ionic column densities in a way that accounts for an absorber that might be inhomogeneous and/or partially covering the background light source, and convert column density ratios to abundance ratios using ionization corrections. In this paper we are going to discuss the first issue, namely the effect of the spatial distribution of ions on the column densities as derived from the observed absorption lines.

A common implicit assumption made when studying absorption line systems in general is that a compact source, such as a star or a quasar, irradiates a cloud whose internal structures are large compared

to the projected size of the continuum source. However, in the more general case, we must consider the two-dimensional distribution of optical depths,  $\tau(x, y, \lambda)$ , across the projected area of the emitting source. The observed residual intensity in an absorption line is then:

$$I(\lambda) = \int \int S(x, y, \lambda) e^{-\tau(x, y, \lambda)} \frac{dxdy}{A}, \quad (1)$$

where  $S(x, y, \lambda)$  is the two-dimensional intensity distribution, emitted by the source at wavelength  $\lambda$ ,  $A = \int \int dxdy$  is the total projected area of the source, and  $\tau(x, y, \lambda)$  is the optical depth distribution across the surface of the continuum emitter. The spatial distribution of the column density per unit wavelength  $\lambda$ ,  $N_\lambda(x, y)$ , is related to  $\tau(x, y, \lambda)$  by:

$$N_\lambda(x, y)d\lambda = \frac{m_e c^2}{\pi e^2 f \lambda^2} \tau(x, y, \lambda) d\lambda, \quad (2)$$

where  $m_e$  is the mass of the electron,  $c$  is the speed of light,  $e$  is the charge of the electron, and  $f$  is the oscillator strength of the line. Hereafter, we will always assume dependence on wavelength, though we will not always indicate it, for the sake of not cluttering the equations below.

Equation (1) expresses the most general situation where the observed spectrum is an intensity-weighted average of  $e^{-\tau(x, y, \lambda)}$  over the projected area of the emitter. The residual intensity in an absorption line depends non-trivially on the optical depth distribution  $\tau(x, y, \lambda)$ . This paper examines a wide range of possible spatial optical depth distributions, characterized for convenience by three functional forms, to study the effects of the shape of the optical depth distribution on the absorption lines, and conversely, on our ability to use the observed absorption lines as diagnostics of the optical depths and column densities in the absorber.

The ionic column density derived from absorption lines depends on how the absorbing cloud covers the continuum source: HPC (Wampler et al. 1995; Barlow, Sargent, & Hamann 1997; Hamann et al. 1997), or inhomogeneous coverage (de Kool, Korista, & Arav 2002). The term *homogeneous* as employed in this paper will always refer to the optical depth being constant across all or part of the spatially extended emission source. We extend the formalism introduced in de Kool et al. (2002), which we will refer to as inhomogeneous partial coverage (IPC), to explore the effects of different variants of inhomogeneous coverage and to compare them with HPC over a wide range of physical conditions. Since we do not know what the optical depth distributions are in real absorbers, it is important to consider a range of possibilities and compare their effects on line strengths and derived column densities. We show how to reparameterize a two-dimensional optical depth distribution to a one-dimensional function in §5 and show that the simple IPC prescriptions we study here provide relatively accurate representations of more complicated distributions.

### 1.1. HPC Analysis

In the spectra of quasar absorption line systems, for example, it has been pointed out that doublet ratios sometimes differ from what one would expect from atomic physics (e.g., Petitjean, Rauch, & Carswell 1994; Wampler, Chugai, & Petitjean 1995; Barlow et al. 1997; Hamann et al. 1997). Hamann et al. (1997) provided an explanation of the ratio discrepancy in terms of a HPC model. In this model, the absorbing cloud covers only a fraction,  $C_f$ , of the continuum source, with the implicit assumption that the coverage fraction for both lines is the same (e.g., see Ganguly et al. 1999; Gabel et al. 2002 for situations when this is not the case). The residual intensities in the doublet lines according to this HPC model are a special case

of Eq. (1), normalized to unity in the continuum:

$$I_s = (1 - C_f) + C_f e^{-\tau_s} \quad (3)$$

for the stronger line, and

$$I_w = (1 - C_f) + C_f e^{-\tau_w} \quad (4)$$

for the weaker line. The  $C_f$ 's and the  $\tau$ 's are also functions of  $\lambda$ . Given  $I_s$  and  $I_w$ , at each wavelength across the profile, for a particular doublet, one can solve simultaneously for the coverage fraction,  $C_f$ , and  $\tau_w = \frac{f_w \lambda_w}{f_s \lambda_s} \tau_s$ , where  $f_s$  and  $f_w$  are the oscillator strengths of the strong and weak lines, respectively, while  $\lambda_s$  and  $\lambda_w$  are wavelengths of the line doublet. Ganguly et al. (1999) gave a general expression for  $C_f$  when  $\tau_s : \tau_w$  is not necessarily 2 : 1. For this special 2 : 1 case, such as for C IV  $\lambda\lambda 1548, 1551$ , Hamann et al. (1997) and Barlow et al. (1997) found that:

$$C_f = \frac{I_w^2 - 2 I_w + 1}{I_s - 2 I_w + 1}, \quad (5)$$

and the optical depth in the stronger line of the doublet is:

$$\tau_s = 2 \ln \left( \frac{1 - I_w}{I_w - I_s} \right). \quad (6)$$

The HPC model uncovered additional layers of complexity in dealing with absorption lines. Barlow et al. (1997) found evidence that the coverage fraction can vary with velocity across the absorption profiles. Arav et al. (1999) discovered an apparent trend between the coverage fraction and the ionization potential of the absorbing ion in the Broad Absorption Line (BAL) QSO PG 0946+301. Another apparent trend was found by Hamann et al. (2001) in which stronger lines seem to have higher coverage fractions. The HPC analysis prompted de Kool et al. (2002) to introduce an inhomogeneous coverage prescription (the IPC, we give a detailed description below). The important difference between the HPC and IPC is the inhomogeneity of coverage. In the IPC formalism the absorbing cloud partially, or sometimes completely, covers the continuum source, but inhomogeneously, i.e. at some locations the optical depth is high, while at others it is low or simply absent. de Kool et al. (2002) parameterized the spatial distribution of optical depths across the surface of the source as a powerlaw in one dimension. Our study will investigate this powerlaw and other parameterizations, provide extensive comparisons with the HPC analysis over a wide range of optical depths, and use the IPC prescriptions directly to derive optical depths from residual intensities synthesized using Eqs. (3) and (4), and develop a formalism to derive properties of the IPC distributions based on the ratios of absorption lines in doublets.

## 2. The IPC Models

A natural question arises in light of the IPC models: What is the effect of the shape of the optical depth distribution on the ionic column densities one measures from the absorption lines, and how do these column densities compare with those derived under the HPC assumption? To address these issues, we first show how an arbitrary optical depth distribution determines the residual intensity level in an absorption line (based on de Kool et al. 2002).

Consider a two-dimensional continuum source with a intensity,  $S(x, y, \lambda)$ , covered with a cloud with an optical depth distribution  $\tau(x, y, \lambda)$ . The resulting residual intensity  $I(\lambda)$  is given by Eq. (1). If the average

emitted intensity is:

$$S_0(\lambda) = \int \int S(x, y, \lambda) \frac{dxdy}{A}, \quad (7)$$

then we can define  $f(\tau, \lambda)d\tau$ , the fraction of the intensity covered by optical depths between  $\tau$  and  $\tau + d\tau$ , as:

$$f(\tau, \lambda)d\tau = \frac{S(x, y, \lambda) dxdy}{S_0(\lambda) A}. \quad (8)$$

If the source has uniform brightness, then the fraction of the area covered by optical depths between  $\tau$  and  $\tau + d\tau$  is:

$$\frac{dxdy}{A} = f(\tau, \lambda)d\tau. \quad (9)$$

With these definitions Eq. (1) reduces to, in normalized units ( $A = 1$ ) and  $S_0 = 1$ :

$$I(\lambda) = \int_{\tau_{min}}^{\tau_{max}} f(\tau, \lambda) e^{-\tau(\lambda)} d\tau, \quad (10)$$

where  $\tau_{max}$  and  $\tau_{min}$  are the maximum and minimum optical depths, respectively, at  $\lambda$ . Without loss of generality, we can rearrange any two-dimensional optical depth distribution to a one-dimensional distribution (see §5) that preserves the fraction of the source (intensity or area) covered at each wavelength. With all these simplifications, the fraction of the area covered by optical depths between  $\tau$  and  $\tau + d\tau$  is  $dx = f(\tau, \lambda)d\tau$ , where  $x$  is a normalized spatial coordinate between 0 and 1.

We consider here three examples for the optical depth distribution. In the first one, the optical depth, or equivalently the column density of some ion, follows a powerlaw distribution in the spatial coordinate  $x$ , as in de Kool et al. (2002). In the second parameterization, the optical depth distribution looks like one quadrant of an ellipse. The third parametrization is a Gaussian distribution. These distribution functions represent an extremely wide range of possible optical depth distributions. The powerlaw and Gaussian are different variations on inhomogeneous complete coverage, while the Ellipse is similar to HPC but with the inclusion of inhomogeneous *partial* coverage (see §2.2). It is worth keeping in mind that HPC is a special case of the IPC analysis where the spatial optical depth distribution involves a step function, a fact which leads to the relatively simple Equations (3) and (4). Our study will go beyond the results presented in de Kool et al. (2002) not only by investigating the Gaussian and Ellipse parameterizations, in addition to the powerlaw, but also by presenting a coherent, easy-to-follow formalism to glean information from absorption line data. The treatment of the powerlaw in this paper will be more general than that in de Kool et al. (2002), in which  $\tau_{min}$  was restricted to zero.

## 2.1. Powerlaw Distribution

With the assumptions taken above, an optical depth described by a powerlaw distribution is then mathematically expressed as:

$$\tau = (\tau_{max} - \tau_{min})x^a + \tau_{min}, \quad (11)$$

where  $\tau_{max}$  and  $\tau_{min}$  are the maximum and minimum optical depths, respectively,  $a$  is the powerlaw index, and  $x$  is a normalized spatial coordinate between 0 and 1. We show examples in Figure 1. A value of  $a = 1$  describes a straight line. The powerlaw index in Eq. (11) is related to the  $p$  parameter in de Kool et al.

(2002) by  $a = 1/(p + 1)$ . For our powerlaw distribution, the fraction of the area covered by optical depths between  $\tau$  and  $\tau + d\tau$  is:

$$dx = \frac{1}{a} \frac{(\tau - \tau_{min})^{(1-a)/a}}{(\tau_{max} - \tau_{min})^{1/a}} d\tau, \quad (12)$$

which corresponds to:

$$f(\tau, \lambda) = \frac{1}{a} \frac{(\tau - \tau_{min})^{(1-a)/a}}{(\tau_{max} - \tau_{min})^{1/a}}. \quad (13)$$

To calculate the residual intensity, we substitute Eq. (13) in Eq. (10) and carry out the integration. The result is:

$$I(\lambda) = \frac{1}{a} \frac{e^{-\tau_{min}}}{(\tau_{max} - \tau_{min})^{1/a}} \Gamma(1/a) P(1/a, \tau_{max} - \tau_{min}), \quad (14)$$

where  $\Gamma$  and  $P$  are the complete and incomplete Gamma functions, respectively. It is important to keep in mind that, in principle, there exist different values of  $\tau_{max}$ ,  $\tau_{min}$ , and  $a$  at every  $\lambda$ . Given a specific optical depth spatial distribution (Eq. 11), Eq. (14) gives the residual intensity at each wavelength across an observed absorption line.

## 2.2. Ellipse Distribution

We will refer to the second optical depth spatial distribution as the ‘‘Ellipse’’. It can be expressed mathematically as:

$$\frac{x^2}{b^2} + \frac{(\tau - \tau_{min})^2}{(\tau_{max} - \tau_{min})^2} = 1, \quad (15)$$

where  $\tau_{max}$  ( $\tau_{min}$ ) are the maximum (minimum) optical depths with  $(\tau_{max} - \tau_{min})$  being the semi-major axis of the ellipse, while  $b$  is its the semi-minor axis. We show in Figure 2 examples for three different  $b$  values. As before, the optical depths and  $b$  are, in principle, functions of wavelength. The Ellipse is similar to the HPC model if  $b < 1$ , with  $b$  playing a role similar to that of  $C_f$ . The fraction of the area covered by optical depths between  $\tau$  and  $\tau + d\tau$  is:

$$dx = - \frac{b}{(\tau_{max} - \tau_{min})} \frac{(\tau - \tau_{min})d\tau}{\sqrt{(\tau_{max} - \tau_{min})^2 - (\tau - \tau_{min})^2}}, \quad (16)$$

where the minus sign only indicates that the optical depth is decreasing with increasing  $x$  (see Figure 2). With this we have:

$$f(\tau, \lambda) = \frac{b}{(\tau_{max} - \tau_{min})} \frac{(\tau - \tau_{min})}{\sqrt{(\tau_{max} - \tau_{min})^2 - (\tau - \tau_{min})^2}}. \quad (17)$$

Following the procedure outlined above, the residual intensity for  $b < 1$  is:

$$I(\lambda) = (1 - b) + \frac{b}{(\tau_{max} - \tau_{min})} \int_{\tau_{min}}^{\tau_{max}} \frac{(\tau - \tau_{min}) e^{-\tau}}{\sqrt{(\tau_{max} - \tau_{min})^2 - (\tau - \tau_{min})^2}} d\tau. \quad (18)$$

For  $b \geq 1$ , we have:

$$I(\lambda) = \frac{b}{(\tau_{max} - \tau_{min})} \int_{\tau_m}^{\tau_{max}} \frac{(\tau - \tau_{min}) e^{-\tau}}{\sqrt{(\tau_{max} - \tau_{min})^2 - (\tau - \tau_{min})^2}} d\tau, \quad (19)$$

where  $\tau_m = \tau_{min} + \frac{(\tau_{max} - \tau_{min})}{b} \sqrt{b^2 - 1}$ . For the  $b \geq 1$  case,  $\tau_m$  (not  $\tau_{min}$ ) is the actual minimum optical depth realized in the absorber (the same also applies for the Gaussian distribution below). These integrals will have to be solved numerically at every  $\lambda$  given  $b$ ,  $\tau_{max}$ , and  $\tau_{min}$ .

### 2.3. Gaussian Distribution

We use a Gaussian as a third example of an optical depth distribution:

$$\tau = (\tau_{max} - \tau_{min}) e^{-\frac{x^2}{2\sigma^2}} + \tau_{min}, \quad (20)$$

where  $\sigma$  is the standard deviation of the Gaussian function (Zombeck 1990). This functional form can describe cases of a small percentage of the maximum optical depth covering a large fraction of the projected area of the continuum source. For instance, if  $\sigma \lesssim 1/3$  and  $\tau_{min} = 0$  then  $\tau \lesssim 0.01\tau_{max}$  over  $\gtrsim (1 - 3\sigma)$  the projected area of the emitter. Distributions for three values of  $\sigma$  are shown in Fig. 3. The covered area is:

$$dx = -\frac{\sigma}{\sqrt{2}} \frac{d\tau}{(\tau - \tau_{min}) \sqrt{\ln \frac{\tau_{max} - \tau_{min}}{\tau - \tau_{min}}}}, \quad (21)$$

where the minus sign is merely due to the arbitrary parameterization (see Figure 3). This area fraction corresponds to:

$$f(\tau, \lambda) = \frac{\sigma}{\sqrt{2}} \frac{1}{(\tau - \tau_{min}) \sqrt{\ln \frac{\tau_{max} - \tau_{min}}{\tau - \tau_{min}}}}. \quad (22)$$

Using the procedure outlined above, we evaluate the residual intensity:

$$I(\lambda) = \frac{\sigma}{\sqrt{2}} \int_{\tau_m}^{\tau_{max}} \frac{e^{-\tau} d\tau}{(\tau - \tau_{min}) \sqrt{\ln \frac{\tau_{max} - \tau_{min}}{\tau - \tau_{min}}}}, \quad (23)$$

where  $\tau_m = (\tau_{max} - \tau_{min}) e^{-1/2\sigma^2} + \tau_{min}$ . It is important to keep in mind that  $\tau_m$  is the minimum optical depth achieved by this distribution. Given  $\sigma, \tau_{max}$ , and  $\tau_{min}$ , we can numerically compute the integral in Eq. (23) to calculate  $I(\lambda)$ .

### 3. Comparisons

In this section, we compare the IPC models to the HPC case as follows. We compute the absorption line intensities and spatially averaged optical depths for different values of  $\tau_{min}$ ,  $\tau_{max}$  and the shape parameters,  $a$ ,  $b$ , and  $\sigma$ , for each of the three IPC distribution functions described above. We use intensities computed for doublets having a 2 : 1 optical depth ratio to derive the coverage fraction and optical depth assuming HPC, based on Equations 3 – 6 in §1. The spatially-averaged optical depth,  $\tau_{avg}$ , for the stronger line in the doublet is:

$$\tau_{avg} = \frac{\int_0^1 \tau dx}{\int_0^1 dx} = \int_0^1 \tau dx. \quad (24)$$

For the powerlaw distribution, this quantity is:

$$\tau_{avg}^{Powerlaw} = \frac{\tau_{max} + a \tau_{min}}{1 + a}, \quad (25)$$

while for the Ellipse ( $b < 1$ ) it is:

$$\tau_{avg}^{Ellipse} = b \tau_{min} + \frac{\pi}{4} b (\tau_{max} - \tau_{min}), \quad (26)$$

and for  $b \gtrsim 1$ :

$$\tau_{avg}^{Ellipse} = \tau_{min} + \frac{\tau_{max}}{b} \left( \frac{\sqrt{b^2 - 1}}{2} + \frac{b^2}{2} \sin^{-1} \frac{1}{b} \right), \quad (27)$$

and for the Gaussian distribution

$$\tau_{avg}^{Gauss} = 1.251 \sigma (\tau_{max} - \tau_{min}) \operatorname{erf}(0.707/\sigma) + \tau_{min}, \quad (28)$$

where “erf” is the Error Function. For the HPC, the spatially averaged optical depth is simply:

$$\tau_{avg}^{HPC} = C_f \tau^{HPC}, \quad (29)$$

where  $\tau^{HPC}$  is the same as  $\tau_s$  in Eq. (6). We plot contour levels, assuming different IPC models, of  $\tau_{avg}^{IPC}/\tau_{avg}^{HPC}$  in Figures 4, 5, and 6 for a set of  $a$ 's,  $b$ 's, and  $\sigma$ 's, with  $\tau_{max}$  taking values between 0.5 and 15 and  $\tau_{min} \leq \tau_{max}$ . We do not plot values for  $\tau_{min} > 5$  because the IPC distributions would describe an opaque slab with complete coverage (or opaque partial coverage for the  $b < 1$  Ellipse distribution). The result would be nearly saturated absorption troughs, and the method for deriving optical depths from the ratio of these troughs would fail.

Notice that a small powerlaw index mimics complete coverage while a large one mimics partial coverage (Fig. 1). For the Ellipse and the Gaussian distributions the situation with  $b$  and  $\sigma$ , respectively, is reversed. (Small values of  $b$  and  $\sigma$  simulate partial coverage, Figs. 2 and 3). A quick glance at Figures 4, 5, and 6 shows that the column densities implied by the HPC doublet analysis are comparable to the average column densities in the IPC distributions used to synthesize the “observed” lines. Notice that, in all cases, the HPC analysis returns precisely the optical depths values of the input IPC distribution when  $\tau_{max} = \tau_{min}$ . Therefore, the dashed diagonal line corresponds to the ratio being  $\tau_{avg}^{IPC}/\tau_{avg}^{HPC} = 1.0$ . The HPC models also asymptotically approach the IPC case for small values of  $a$  and large values of  $b$  and  $\sigma$ , as is apparent from Figures. 1, 2, and 3. In these cases, all of the IPC models actually resemble complete homogeneous coverage. An interesting situation occurs for the Ellipse distribution. When the semi-minor axis is less than 1, this HPC model becomes very similar to the IPC, especially for  $\tau_{min} \approx \tau_{max}$  (Figs. 2 and 5).

The contours in Figures 4, 5, and 6 run more or less parallel to the dashed diagonal line. Qualitatively, why do the contours behave the way they do? To answer this question, choose any IPC model and pick the plot corresponding to some specific  $a$ ,  $b$ , or  $\sigma$ , as the case might be. At a particular  $\tau_{max}$ , as  $\tau_{min}$  increases the distribution shape (Figs. 1 – 3) begins more and more to resemble that of a homogeneously, completely covering cloud for the Gaussian and powerlaw distributions, or a homogeneous partial coverage for the Ellipse. In either case, in terms of average optical depths, the HPC output is nearly identical to the IPC input, and hence the ratio decreases from its maximum value when  $\tau_{min} = 0$  to unity as  $\tau_{min}$  approaches  $\tau_{max}$ . This decrease is most rapid for peaked optical depth distributions, and hence the closely spaced contours. Sharply peaked distributions also lead to the largest differences between the ionic column densities in the IPC distribution and those derived under the HPC assumption. The decrease in ratio is less dramatic for optical depth distributions that more uniformly cover the source, and hence lead to contours that are close to unity, such as all the Ellipse clouds, the large  $\sigma$  Gaussians, and the small  $a$  powerlaws. As a matter of fact, the Ellipse clouds are always very similar to the HPC.

The HPC results differ most dramatically from the IPC input when the IPC distribution is sharply peaked (large  $a$  for the powerlaw or small  $\sigma$  for the Gaussian) and there is a transition across this distribution from very optically thick ( $\tau_{max} \gg 1$ ) to optically thin ( $\tau_{min} \approx 0$ ). For example, the parameters  $a = 10$ ,  $\tau_{min} = 0$ , and  $\tau_{max} = 15$  in the powerlaw distribution (Eq. 11) lead to a spatially-averaged optical depth of

$\tau_{avg}^{Powerlaw} = 1.4$ . Also  $\sim 24\%$  of the source is covered by regions having  $\tau > 1$ . An HPC analysis applied to the absorption doublets generated by this particular IPC distribution yields a  $C_f = 0.29$ , which, as expected, is similar to the  $\sim 24\%$  of the source covered by  $\tau > 1$  gas in the actual distribution. The optical depths inferred from the HPC analysis are  $\tau^{HPC} = 2.9$  for lines of sight hitting the absorber, and zero elsewhere, implying a spatially-averaged optical depth of  $\tau_{avg}^{HPC} = 0.84$ . We show in Figs. 7, 8, and 9 the results of similar calculations for the powerlaw, Ellipse, and Gaussian distributions, respectively. The horizontal lines are the values of the corresponding  $\tau_{avg}^{IPC}$  and  $\tau_{avg}^{HPC}$ .

It is not surprising that  $\tau_{avg}^{HPC}$  in the previous paragraph is less than  $\tau_{avg}^{Powerlaw}$  in the actual powerlaw distribution. The reason is that the absorption line strength is not sensitive to the exact value of  $\tau$  in regions where  $\tau$  is already  $\gg 1$ , e.g., on the right-hand side of Fig. 1a. For example, if we keep the same  $\tau(x)$  distribution but truncate the peak at  $\tau = 10$  or even  $\tau = 5$ , we would lower the value of  $\tau_{avg}^{Powerlaw}$  without significantly affecting the absorption line strengths. Similarly, adding material (to increase the optical depth) in regions where  $\tau$  is already  $\gg 1$  could increase  $\tau_{avg}^{Powerlaw}$  arbitrarily, but there would again be no change in the amount of absorption as registered by the absorption lines.

The HPC analysis is remarkably accurate when applied to optical depth distributions that do not contain sharp spikes, i.e., having areas with  $\tau \gg 1$ , because the absorption lines themselves are not sensitive to optical depths in the  $\tau \gg 1$  regions. Without specific knowledge of the true shape of the optical depth distribution, there is no prospect of using measured absorption lines to estimate the amount of material (column density) that might be present in very optically thick regions. However tighter constraints could be obtained by using, not just doublets with 2 : 1 ratios, but multiplets and lines of more/less abundant ions that span a much wider range in  $\tau$ .

#### 4. Applications

The IPC models can also be applied to observed absorption line doublets (or multiplets) to derive key parameters of the optical depth distribution. To illustrate this, we use the HPC model, Eqs. (3) and (4) given  $C_f$  and  $\tau_s$ , to simulate “observed” residual intensities,  $I_s$  and  $I_w$ , in doublet lines whose optical depths are in a 2 : 1 ratio. Basically, we follow the reverse approach of the previous section: we now assume that the doublet created with the HPC model is the “observed” and we solve for  $\tau_{max}$  and  $a$ ,  $b$ , or  $\sigma$ . (We fix  $\tau_{min} = 0$ , with a little loss of generality, to reduce the number of unknowns in our equations). For every functional form of IPC, we get two equations with two unknowns (see Eqs. (14), (18), (19), and (23)), which we solve numerically using Newton’s method (Press et al. 1992). The success of this approach hinges on providing a good initial guess. We find that trial and error guesses at  $\tau_{max}$  and the shape parameter, guided by the input HPC values  $C_f$  and  $\tau^{HPC}$ , lead more quickly to the best solution. The implementation of Newton’s method also allowed us to confirm that the solutions arrived at are unique and not local minima which the numerical code converged to by mistake.

The aim behind this exercise is to prove the feasibility of our IPC models in solving simultaneously, just as in the HPC case, for the optical depth and the “shape” parameter. We also note parenthetically that one can arrive back at the HPC input values if one uses the derived IPC parameters to simulate the residual intensities and then apply the HPC doublet analysis. This shows that the IPC doublet analysis we present in this section is reliable. We test our method for a range of HPC parameters that would reveal the representative behavior of the solutions. Table 1 lists combinations of  $C_f$  and  $\tau^{HPC}$ , used as input, and corresponding derived values of  $\tau_{max}^{IPC}$ ,  $a$ ,  $b$ , and  $\sigma$ . We chose three values of  $\tau^{HPC} = 0.5, 1.0, \text{ and } 5.0$ , to



span the range from optically thin to optically thick. The average optical depths are calculated using Eqs. (25), (26), (27), (28), and (29). For  $C_f$  we chose 0.1, 0.5, and 0.9 to investigate the effects of the degree of partial coverage on the resulting IPC solutions.

We compare the various quantities in Table 1. It is interesting to see how very low coverage leads to very large powerlaw indices and large derived values of  $\tau_{max}$ . For low optical depths with HPC the resulting maximum optical depth derived under the powerlaw IPC is about a factor of two larger. But the optically thick case ( $\tau^{HPC} = 5.0$ ) with low coverage ( $C_f = 0.1$ ) is much more extreme. We can understand this behavior because the powerlaw distribution describes complete coverage. It therefore strains to mimic a partial coverage situation with large  $a$  values, resulting in a large spike in  $\tau(x)$ . This spike dominates  $\tau_{avg}$ , but it is purely an artifact of the functional form. It shows that the powerlaw distribution IPC is completely unreliable in this regime. One can always truncate the maximum optical depth value at some very high value without affecting strength of the resulting absorption lines.

A quick glance at the Ellipse solutions, both in terms of  $\tau_{max}$  and  $\tau_{avg}$ , shows that this IPC model is very similar to HPC (cf. previous section). On the other hand, the Gaussian distribution behaves like a combination of the powerlaw, in terms of the peakedness, and the Ellipse. The Gaussian, like the powerlaw, is based on complete coverage. But the rapid decline in the Gaussian distribution from the core to the wings (Fig. 3) is better able to mimic partial coverage. Nonetheless, like the powerlaw case, optically thick clouds with small coverage fractions can lead to solutions with artificially large spikes in the Gaussian  $\tau(x)$ . We see that the derived average optical depths with the powerlaw, Ellipse, and Gaussian distributions are comparable to the average optical depth used to generate the HPC input, with the exception of the optically thick case  $\tau^{HPC} = 5.0$ .

The doublet analysis provides a shape parameter and  $\tau_{max}$ . But we are forced to assume a functional form that substantially affects the results (Table 1). Working with multiplets with “n” lines, or any combination of “n” lines whose  $\tau$ 's can be reliably tied together, would provide “n” equations and “n” unknowns and therefore “n” constraints on the two-dimensional optical depth distribution. Such complicated procedure is, however, beyond the scope of this paper.

## 5. Two-Dimensional Optical Depth Distributions

We describe in this section a procedure to re-parameterize an arbitrary two-dimensional optical depth distribution,  $\tau(x, y)$ , into a one-dimensional function  $\tau(x)$ . We show that the simple functional forms discussed above are relatively successful at representing more realistic and complicated situations. Our starting point is to create an arbitrary 2D optical depth distribution. This 2D distribution, for the sake of definiteness but with some loss of generality, is the surface made from a collection of 36 overlapping Gaussian functions scattered over a plane (Fig. 10). The positions and heights of the Gaussian functions are chosen randomly, with numbers between 0 and 1 for the abscissae/ordinates and between 0 and 3 for the heights (peak optical depths for the individual Gaussians). We pick the same Gaussian width,  $\sigma = 0.06$ , for all the functions so as not to get very narrow or very wide spatial profiles. The outcome of this process is a 2D optical depth distribution across the surface of an emitter, which we assume to be emitting uniformly. The maximum optical depth in this distribution is  $\tau_{max} = 6.42$ , the minimum optical depth is  $\tau_{min} = 0.0018$ , and the average is  $\tau_{avg} = 1.17$ .

We then calculate the fraction of the area covered by optical depths between  $\tau$  and  $\tau + d\tau$ . We divide the surface into a grid of 2D cells and count the number of cells with optical depths between  $\tau$  and  $\tau + d\tau$ .

This gives us  $f^{2D}(\tau, \lambda)$  for our 2D distribution. It is now straightforward to integrate this function (recall  $dx = (f(\tau, \lambda)d\tau)$ ) to get the equivalent 1D optical depth distribution  $\tau(x)$ . We show the results in Figure 11 (solid line).

To calculate the residual doublet (with 2 : 1 ratio) line intensities from such a distribution we numerically substitute  $f^{2D}(\tau, \lambda)$  in Eq. (10) and evaluate the integral. This gives us two “observed” residual intensities for the doublet lines. We then apply our HPC and IPC analyses to this “observed” doublet to solve for the shape parameters and  $\tau_{max}$ , putting  $\tau_{min} = 0$  in the IPC case. We show the results in Table 2. The average optical depths calculated with all of the HPC and IPC models are comparable to the average optical depth in the original 2D distribution. This shows that the relatively simple functional forms we discussed in this paper provide practical representations to describe a complicated optical depth distribution.

We plot the corresponding HPC and IPC optical depth distributions in Figure 11 for comparison with the equivalent 1D distribution. It is easy to see that the powerlaw and Gaussian functional forms are the closest to the re-parameterized 1D distribution, which was created from overlapping Gaussians. This re-parameterized 1D function is more sharply peaked than the 1D IPC powerlaw that we derive from the doublet analysis. This shows that spikes in  $\tau(x)$  can arise naturally from “real” 2D distributions, even if those distributions are based on a very simple, non-spikey function (a Gaussian). The “spikeness” in the 1D re-parameterization (Fig. 11) is the result of having few peaks in the 2D distribution (Fig. 10).

## 6. Conclusions

Understanding the effects of the spatial distribution of ions in an absorbing region is essential to deciphering the physical and chemical states of the absorber. Our investigations of the effects of the spatial distribution of ions in an absorbing region on the derived column densities reveal a number of interesting properties. So long as an absorbing region is not optically thick we find that the average optical depth of the input distribution, i.e., the one used to generate the “observed” residual intensities in an absorption doublet, will lead to a comparable, to within a factor of less than 1.5, average optical depth derived from a doublet analysis assuming a different optical depth distribution. Figures 4, 5, and 6 along with Tables 1 and 2 attest to this. In Figures 4, 5, and 6 we start with an IPC distribution,  $\tau_{max}$ ,  $\tau_{min}$ , and the appropriate shape parameter, and then derive  $\tau^{HPC}$  and  $C_f$  for the HPC case. We plot the ratio of the average optical depths,  $\tau_{avg}^{IPC} / \tau_{avg}^{HPC}$ , as contours, whose values are always less than  $\sim 1.6$  in the part of parameter space we study.

Table 1 shows the results of the reverse approach. We start by simulating an absorption doublet using an HPC distribution as input and use an IPC distribution to calculate the attributes of the absorbing region. It is easy to see that  $\tau_{avg}^{HPC} \approx \tau_{avg}^{IPC}$ , except in the optically thick regime. We also should point out that we can get back to the initial HPC parameters from the IPC solutions by following the same approach employed of Figures 5, 6, and 7. This symmetry proves that our IPC doublet analysis method is reliable. We have extended the work of de Kool et al. (2002) to show how, given a functional form in the IPC analysis, we can use observed lines (e.g., doublets) to infer key parameters about the inhomogeneous optical depth and column density distributions.

We go a step further in §5 (Table 2). We start with an arbitrary 2D optical depth distribution and calculate the resulting doublet residual intensities, which we then analyze with the HPC and IPC models. The last column in Table 2 shows that the resulting average optical depths are almost identical to the average optical depth of the initial 2D distribution. All this discussion leads us to an important conclusion: Our investigation shows that the spatial distribution of ions has a minimal effect on the computed average column

density. Given the fact that spikes could arise from not so exotic 2D distributions (Figs. 10 and 11) and that the re-parameterized 1D function is closest to a powerlaw (Fig. 11), we conclude that the IPC powerlaw doublet analysis should yield more representative parameters of the absorbing line region. Solving Eq. (14) for a doublet that provides two equations in two unknowns ( $\tau_{max}$ ,  $a$ , with  $\tau_{min} = 0$ ), is relatively easy. In a future paper we will apply our methods to observed quasar absorption lines and present the numerical codes that implement our IPC doublet analysis.

*Acknowledgements:* We wish to acknowledge support through NSF grant AST99-84040.

## REFERENCES

- Barlow, T. A., Hamann, F., & Sargent, W. L. W. 1997, in ASP Conf. Series 128, Mass Ejections from AGN, ed. R. Weymann, I. Shlosman, & N. Arav (San Francisco: ASP), 13
- de Kool, M., Korista, K. T., & Arav, N. 2002, ApJ, 580, 54
- Gabel, J. R., et al. 2003, ApJ, in press
- Ganguly, R., Eracleous, M., Charlton, J. C., Churchill, C. W. 1999, AJ, 117, 2594
- Hamann, F., Barlow, T. A., Junkkarinen, V., & Burbidge, E. M. 1997, ApJ, 478, 80
- Hamann, F., & Ferland, G. 1999, ARA&A, 37, 487
- Hamann, F., Barlow, T. A., Chaffee, F. C., Foltz, C. B., & Weymann, R. J. 2001, ApJ, 550, 142
- Petitjean, P., Rauch, M., & Carswell, R. F. 1994, A&A, 291, 29
- Press, W. H., Teukolsky, S. A., Vetterlin, W. T., & Flannery, B. P. 1992, Numerical Recipes in Fortran: The Art of Scientific Computing, Second Edition, (Cambridge, UK: Cambridge University Press)
- Verner, D. A., Barthel, P. D., & Tytler, D. 1994, A&AS, 108, 287
- Wampler, E. F., Chugai, N. N., & Petitjean, P. 1995, ApJ, 443, 586
- Zombek, M. V. 1990, Handbook of Astronomy and Astrophysics, Second Edition (Cambridge, UK: Cambridge University Press)

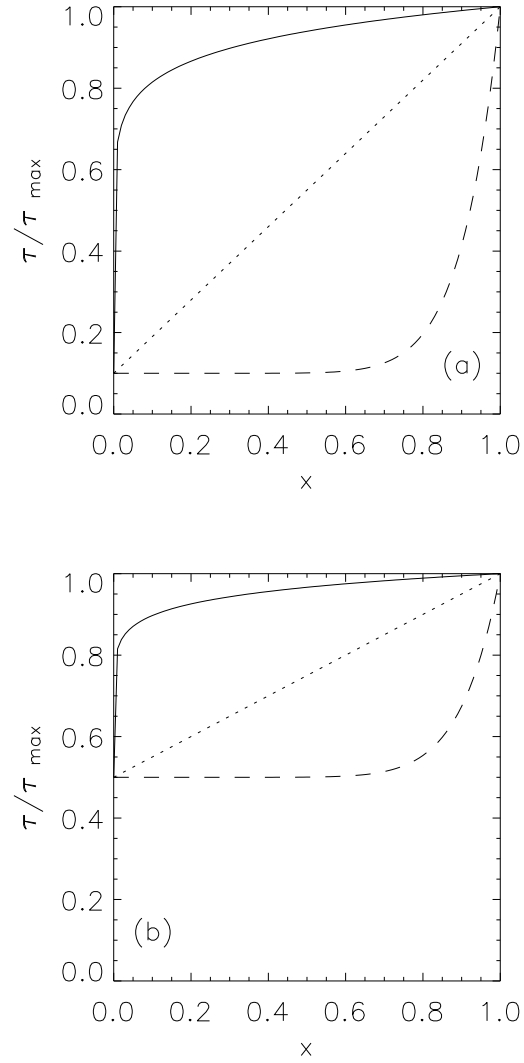


Fig. 1.— Powerlaw distribution with  $\tau_{\min} = 0.1 \tau_{\max}$  (a) and  $\tau_{\min} = 0.5 \tau_{\max}$  (b). Solid, dotted, and dashed lines for  $a = 0.1, 1.0$ , and  $10$ , respectively.

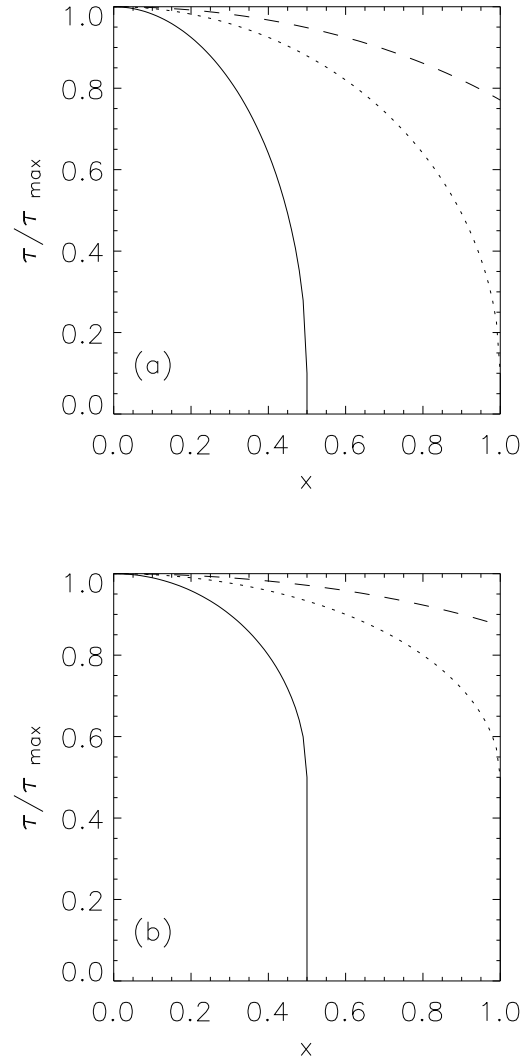


Fig. 2.— Ellipse distribution with  $\tau_{\min} = 0.1 \tau_{\max}$  (a) and  $\tau_{\min} = 0.5 \tau_{\max}$  (b). Solid, dotted, and dashed lines for  $b = 0.5, 1.0$ , and  $1.5$ , respectively.

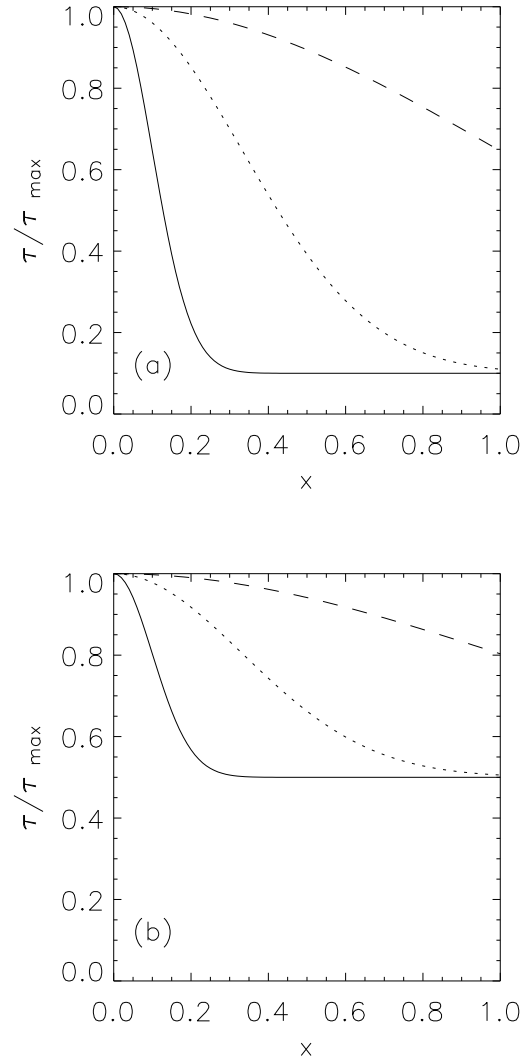


Fig. 3.— Gaussian distribution with  $\tau_{\min} = 0.1 \tau_{\max}$  (a) and  $\tau_{\min} = 0.5 \tau_{\max}$  (b). Solid, dotted, and dashed lines for  $\sigma = 0.1, 0.33$ , and  $1.0$ , respectively.

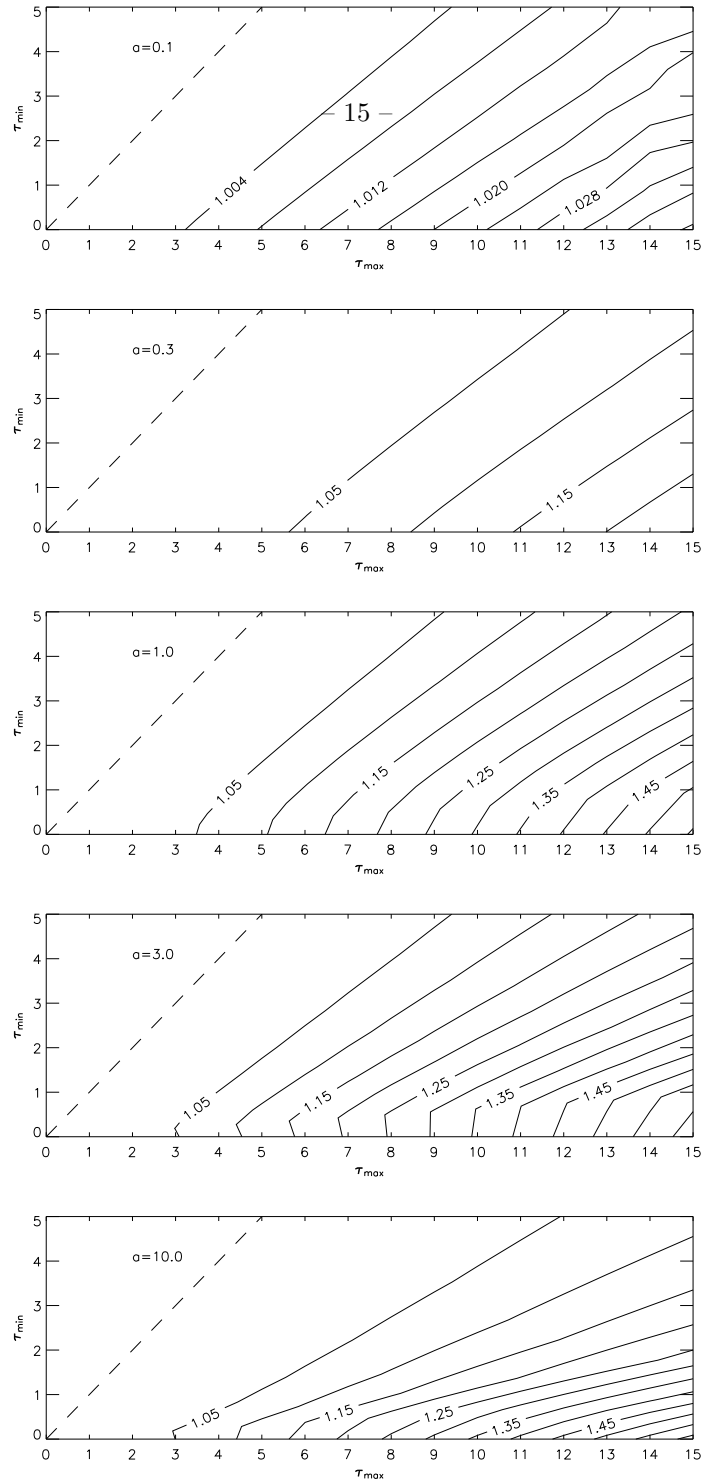


Fig. 4.— Powerlaw Distribution vs. HPC. Contours show the ratio of spatially-averaged optical depths calculated in the IPC model to that computed under HPC assumptions, i.e.,  $\tau_{avg}^{IPC} / \tau_{avg}^{HPC}$ . The dashed curve indicates  $\tau_{min} = \tau_{max}$ , which also corresponds to  $\tau_{avg}^{IPC} / \tau_{avg}^{HPC} = 1$ , because in this limit, the  $\tau(x)$  distribution (Eq. 11) is homogeneous.

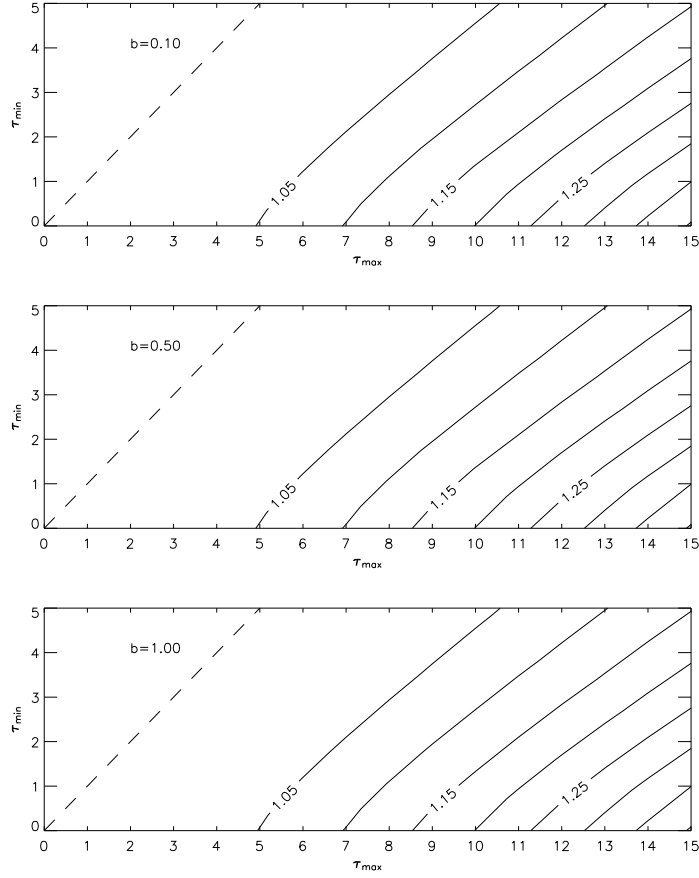


Fig. 5.— Same as Fig. 4 but for Ellipse Distribution vs. HPC. For  $b > 1.0$ , IPC model is the same as homogeneous, complete coverage, and hence the ratio of optical depths is always 1.

Table 1: IPC Solutions

$C_f, \tau_{HPC}^{HPC}, \tau_{avg}^{HPC}$	$a, \tau_{max}^{Powerlaw}, \tau_{avg}^{Powerlaw}$	$b, \tau_{max}^{Ellipse}, \tau_{avg}^{Ellipse}$	$\sigma, \tau_{max}^{Gaussian}, \tau_{avg}^{Gaussian}$
0.1, 0.5, 0.05	20.1, 1.1, 0.05	0.14, 0.4, 0.04	0.06, 0.67, 0.05
0.1, 1.0, 0.10	22.1, 2.4, 0.10	0.10, 1.1, 0.09	0.05, 1.43, 0.09
0.1, 5.0, 0.50	832, 3415, 4.10	0.10, 6.9, 0.54	0.04, 36.4, 1.82
0.5, 0.5, 0.25	2.6, 0.9, 0.25	0.70, 0.4, 0.22	0.29, 0.65, 0.24
0.5, 1.0, 0.50	2.9, 2.0, 0.51	0.55, 1.2, 0.52	0.27, 1.43, 0.48
0.5, 5.0, 2.50	9.6, 444, 41.8	0.51, 6.9, 2.76	0.18, 36.4, 8.19
0.9, 0.5, 0.45	0.5, 0.7, 0.47	1.18, 0.5, 0.46	0.54, 0.69, 0.44
0.9, 1.0, 0.90	0.6, 1.4, 0.87	1.00, 1.1, 0.86	0.66, 1.19, 0.85
0.9, 5.0, 4.50	1.4, 20.4, 8.5	0.91, 6.9, 4.90	0.33, 36.4, 15.0



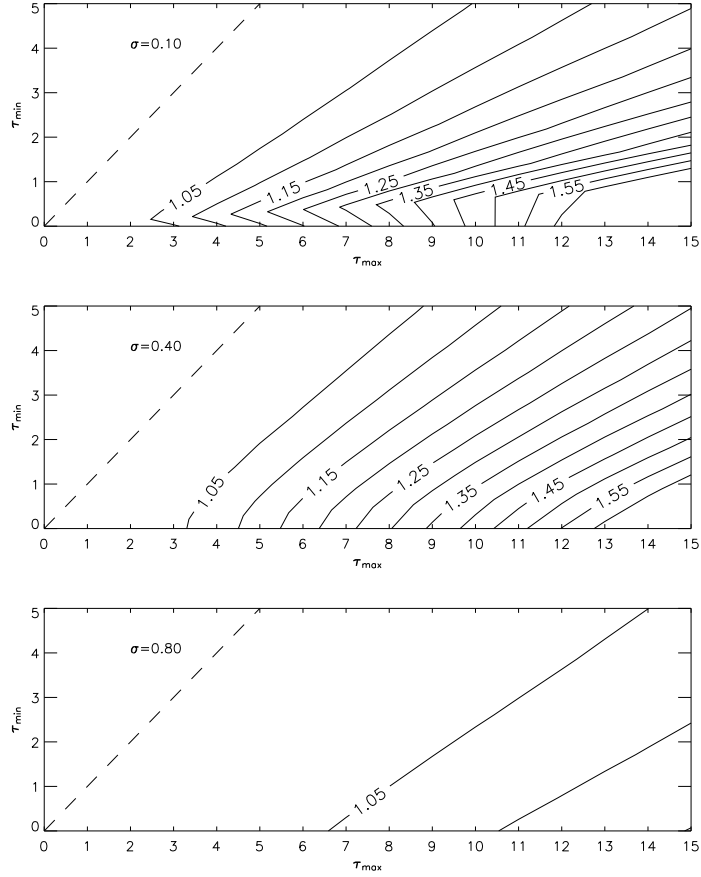


Fig. 6.— Same as Fig. 4 but for Gaussian Distribution vs. HPC. For  $\sigma > 0.8$ , IPC model is the same as homogeneous, complete coverage, and hence the ratio of optical depths is always 1.

Table 2: 2D Distribution & HPC/IPC Models

Model	Geometry	$\tau_{max}$	$\tau_{avg}$
2D	—	6.42	1.17
HPC	0.66	1.60	1.06
Powerlaw	1.86	3.18	1.11
Ellipse	0.70	1.90	1.05
Gaussian	0.34	2.54	1.08

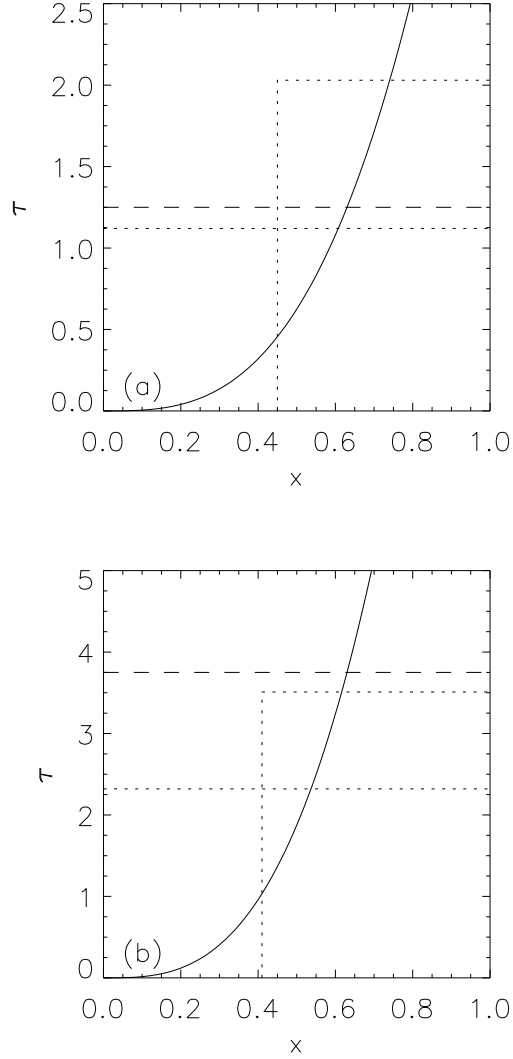


Fig. 7.— Powerlaw distribution for  $a = 3$  (solid curves) with  $\tau_{max} = 5$  (top panel) and  $\tau_{max} = 15$  (bottom). The dashed horizontal lines show the average optical depth,  $\tau_{avg}^{IPC}$ , of these distributions. The dotted rectangles show the HPC distributions of the optical depths, as derived from the doublet analysis using the IPC distributions as input (see §3). The horizontal dash-dotted lines mark the values of  $\tau_{avg}^{HPC}$ , the average optical depths of the HPC distributions. The plots were truncated at  $\tau < \tau_{max}$  to aid in noticing the differences between the average optical depths.

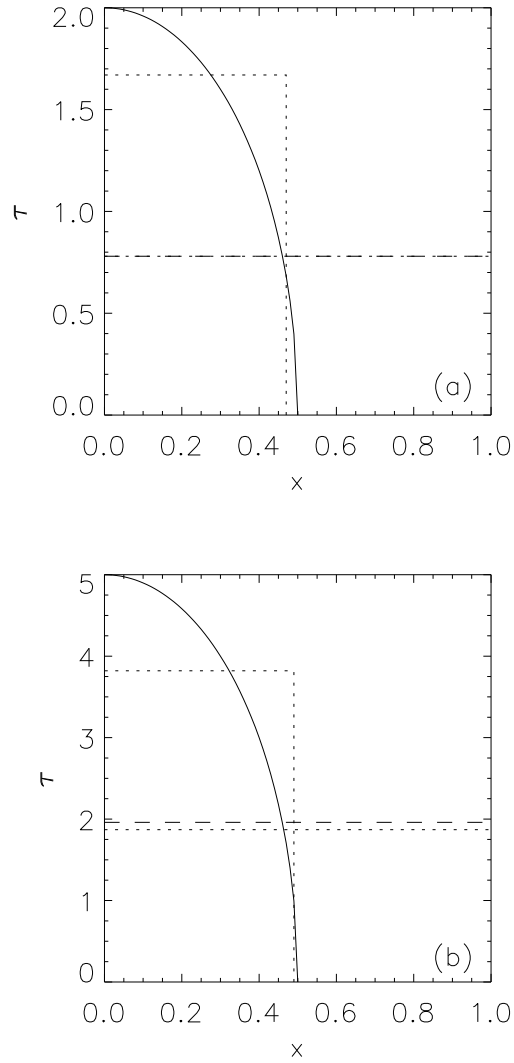


Fig. 8.— Same as for Fig. 7 but for an Ellipse distribution ( $b = 0.5$ ) with  $\tau_{max} = 2$  (top, a), and  $\tau_{max} = 5$  (bottom, b). We chose lower optical depth values to avoid black troughs.

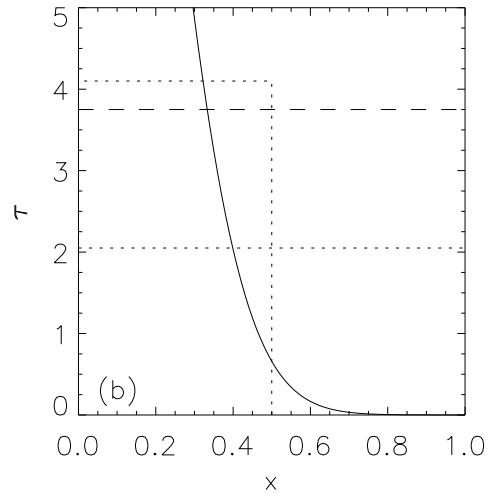
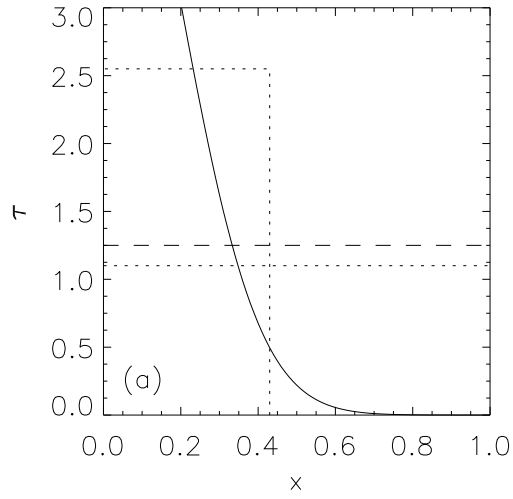


Fig. 9.— Same as for Fig. 7 but for an Gaussian distribution with  $\sigma = 0.2$  with  $\tau_{max} = 5$  (top, a), and  $\tau_{max} = 15$  (bottom, b).

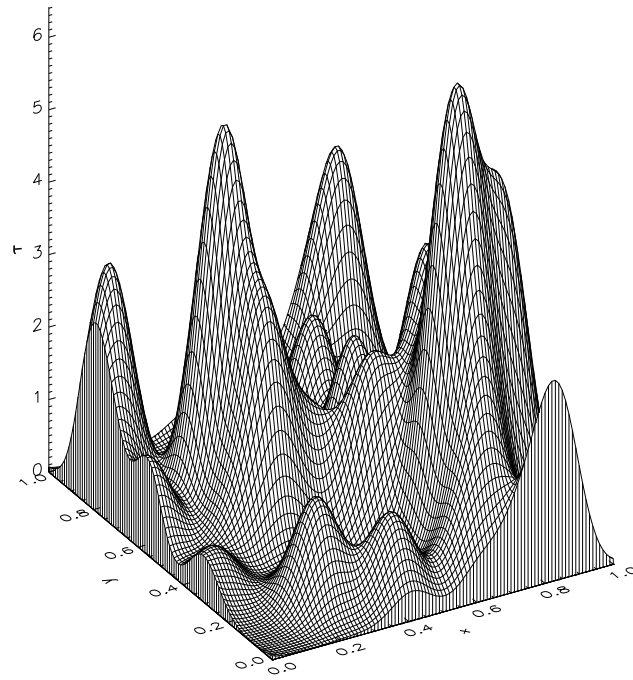


Fig. 10.— Two dimensional optical depth distribution synthesized from 36 overlapping Gaussians.

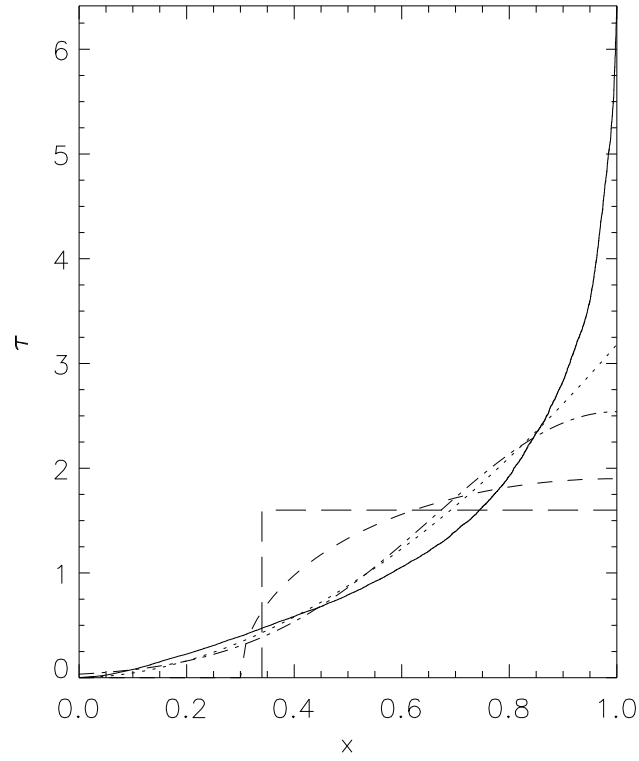


Fig. 11.— The 1D re-parameterization (solid curve) of the 2D optical depth distribution shown in Figure 10 is shown with the powerlaw (dotted), Ellipse (dashed), Gaussian (dash-dotted), and HPC (long dashed) distributions derived for the doublet analysis in (§5).